Effects of Molecular and Electronic Structures in CoO$_x$/CeO$_2$ Catalysts on NO Reduction by CO

Shuhao Zhang,[†] Yuanyuan Li,[†] Jiahao Huang,[†] Jaeha Lee,[‡] Do Heui Kim,[‡] Anatoly I. Frenkel,[†,§] and Taejin Kim*,[†]

[†]Materials Science and Chemical Engineering Department, Stony Brook University, Stony Brook, New York 11794, United States
[‡]School of Chemical and Biological Engineering, Institute of Chemical Processes, Seoul National University, Seoul 08826, Republic of Korea
[§]Chemistry Division, Brookhaven National Laboratory, Upton, New York 11973, United States

S *Supporting Information*

ABSTRACT: Ceria-supported transition metal oxide (such as CoO$_x$) catalysts are promising, more cost-effective candidates to replace platinum group metal catalysts in the NO reduction process. A series of CoO$_x$ (0.2−31.3 Co/nm^2) catalysts supported on CeO$_2$ were prepared by the incipient wetness impregnation method and were tested for NO reduction by CO reaction in this work. Various characterization techniques, including Brunauer−Emmett−Teller, Raman spectroscopy, powder X-ray diffraction (XRD), X-ray absorption spectroscopy (XAS), and diffuse reflectance infrared Fourier transform spectroscopy (DRIFTS) were used to investigate the molecular and electronic structures of CoO$_x$/CeO$_2$ catalysts. It was observed that there are structural changes with varied Co loadings, such as (1) sub-monolayer: <2.3 Co/nm^2, (2) monolayer: 2.3−2.7 Co/nm^2, and (3) over-monolayer: >2.7 Co/nm^2. The highest molar rate was observed at the 2.7 Co/nm^2 sample. In the case of over-monolayer samples, such as 7.1 Co/nm^2, the oxidation state of Co affected the catalytic activity. Using in situ XAS, an oxidation state change from Co^{3+} to Co^{2+} between 200 and 300 °C was identified. Catalyst deactivation was also affected by the change of Co oxidation states from the fresh sample (Co^{3+}) to the used sample (Co^{3+}/Co^{2+}). N$_2$O formation and decomposition were affected by the reaction temperature in a two-step procedure, where NO converts into N$_2$: (1) NO → N$_2$O and (2) N$_2$O → N$_2$. N$_2$ selectivity monotonically increased with an increasing reaction temperature between 200 and 400 °C. The results provided several structure−property relationships and a possible reaction mechanism for NO reduction by CO reaction over CoO$_x$/CeO$_2$ catalysts.
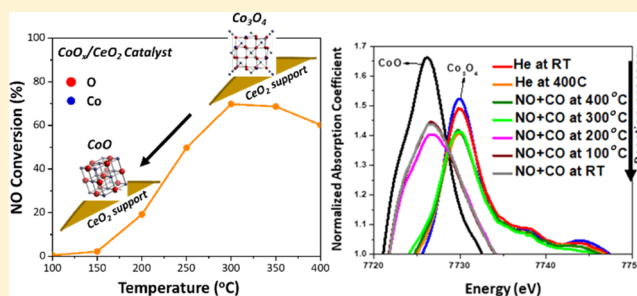
1. INTRODUCTION

Anthropogenic greenhouse gas emissions and pollutants in the atmosphere are causing growing global warming concerns.[1] Nitrogen oxides (NO$_x$) are some of the main contributors—in addition to hydrocarbons (HCs), carbon monoxide (CO), sulfur oxides (SO$_x$), and particulate matters—to air pollution.[2−6] Many investigations have been performed for catalytic NO$_x$ (mainly NO) reduction, resulting in the development of techniques, such as NO reduction by hydrocarbon or CO and NH$_3$-selective catalytic reduction.[7−12] Among the discovered methods, NO reduction by CO (2NO + 2CO → N$_2$ + CO$_2$) has received much attention because a large amount of carbon monoxide (CO) also exists in automobile exhausts. Because CO is also one of the notorious pollutants, the reduction of NO by CO is an important approach that can reduce two pollutants (NO and CO) simultaneously. Moreover, this is a major catalytic reaction in three-way catalytic converters (TWCs). For the past few decades, supported platinum group metals (PGMs), such as Pt, Rh, Ru, and Pd, have been

used in the NO reduction by CO reaction due to their high activity and high resistance to catalyst deactivation.[13−17] It has been suggested that the NO reduction by CO reaction is a two-step reaction: CO + 2NO → N$_2$O + CO$_2$ (nitrous formation) and CO + N$_2$O → N$_2$ + CO$_2$ (nitrous reduction).[18] The NO reduction by CO is also believed to be a site-specific reaction, including CO adsorption and NO dissociation.[19] N$_2$O is a product from incomplete NO reduction, especially during the cold start period of vehicles. Due to the fact that N$_2$O is very difficult to remove, the N$_2$O dissociation rate and N$_2$ selectivity should be improved to satisfy the NO$_x$ regulation. The important roles of metal−support and metal−oxygen-support interactions have also been emphatized in the literature.[20−22] Granger et al. reported that different supports could control the rate constant of two

competitive steps, such as $2N^* \rightarrow N_2 + 2^*$ and $N^* + NO^* \rightarrow N_2O + 2^*$, where * is a vacant adsorption site.[23] Pt (or Pd)/CeO_2 showed higher NO reduction compared to Al_2O_3 supported catalysts because of their strong metal−ceria interaction and the formation of solid solution, $Ce_{1-x}M_xO_2$.[24] Mono- and bimetallic supported catalysts have also been investigated to improve the catalytic activity and N_2 selectivity. For example, Schmal et al. reported that Pd−Mo/Al_2O_3 catalysts showed higher N_2 formation than that of the Pd/Al_2O_3 catalysts.[25] The authors also observed the change of oxidation states of Pd and Mo (e.g., Pd^{2+}, Pd^0, Mo^{6+}, and $Mo^{\delta+}$) during the NO reduction by CO reaction and concluded that $Mo^{\delta+}$ promotes catalytic activity and N_2 selectivity.

From an economic point of view, the use of PGMs should be reduced due to their high cost and scarcity.[26] Therefore, much attention has been paid to explore the supported transition metal oxide catalysts, which have shown promising results for N_2O decomposition and CO oxidation.[27−32] Among transition metals, cobalt is a great candidate as a replacement for noble metals because of its abundance, low cost, and high stability under harsh reaction conditions.[33,34] Considering these factors, cobalt oxide (CoO_x) has been studied and used as a heterogeneous catalyst in several chemical reactions like CO oxidation, water−gas shift, dry reforming, ethanol steam reforming, and soot combustion.[35−39] Recently, An et al. reported that Co_3O_4 loaded with Pt nanoparticles showed higher CO oxidation activity under reducing conditions than other mesoporous oxides, such as NiO, MnO_2, and FeO_2.[40] The authors also found that the Co^{2+} site is the active site in the Pt/Co_3O_4 catalyst, whereas octahedrally coordinated surface Co^{3+} is the active site in bulk Co_3O_4. In addition, the oxidation state of CoO_x during the CO oxidation reaction has been investigated by in situ spectroscopic techniques, such as the X-ray absorption near edge structure (XANES) and ambient-pressure X-ray photoelectron spectroscopy (XPS) by Jansson et al.[41] They found that the catalyst deactivated as surface cobalt oxide reconstruction occurred. Also, the deactivated catalyst could be reactivated by oxidizing procedures. These results imply that the oxidation state of CoO_x plays a key role in controlling the catalytic activity in NO reduction by CO reaction.

Ceria is widely used as an oxide support in the TWCs because it has shown outstanding redox ability (Ce^{4+}/Ce^{3+}), high oxygen storage capacity, high dispersion of noble metals, and the ability to improve the thermal stability when combined with other metal oxides.[42−46] It has been reported that the combination of ceria with transition metal oxide (or metal) improved redox properties and surface oxygen mobility, which resulted in higher catalytic activity during the NO reduction by CO reaction.[47] Deng et al. reported that pure CeO_2 showed no activity for the CO oxidation and very low activity for the NO reduction by CO reaction up to 300 °C.[30] However, Mn-doped CeO_2 and Cu/CeO_2 catalysts showed improved catalytic activities for both CO oxidation and NO reduction by CO reaction, although CO conversion was still low (∼50%). Using ex situ XPS and in situ DRIFT results, the authors claimed that the catalytic activity is directly related to Ce^{3+}, oxygen vacancies, and ceria cell lattice expansion. Liu et al. also observed higher photocatalytic NO reduction by CO reaction activity over the CuCeTi catalyst compared to the CuTi catalyst using in situ diffuse reflectance infrared Fourier transform spectroscopy (DRIFTS).[48] The authors hypothe-

sized that the transferred oxygen from ceria to copper increased oxygen vacancies and oxygen concentrations in ceria and copper, respectively. This transition of oxygen resulted in higher catalytic activity during the NO reduction by CO reaction. It is well documented that the loading of surface species (e.g., metal oxide) can affect the catalytic activity and molecular structure, so the determination of monolayer coverage is very important because the monolayer sample should contain the highest dispersion of surface species on the support without forming a crystalline structure.[49−51] Recently, Savereide et al.[52] also studied the effect of CeO_2 morphology in CoO_x/CeO_2 catalysts for the NO + CO reaction and noticed that, compared to nanoparticles and nanocubes, the CeO_2 nanorod has a rougher surface and more oxygen vacancy defects. These features help charge transfer on the metal−support interface as well as keep Co oxidation states stable during reaction conditions. As a result, the authors found that cobalt oxide catalysts with CeO_2 nanorods as the supporting material performed better in the NO + CO reaction than the ones with CeO_2 nanoparticles or nanocubes as supports.

For the reasons briefly summarized above, the CoO_x/CeO_2 catalyst has been used in several reactions and processes like steam reforming[53,54] and N_2O decomposition.[55] It has been proven in these studies that the CoO_x/CeO_2 catalyst is a very promising catalyst to replace PGMs due to its high activity and good stability. However, a systematic understanding of the fundamental molecular structure of the catalyst and the structure−activity relationship for the NO reduction by CO reaction is lacking. For instance, the changes in molecular structures with different Co loadings, as well as the changes of the oxidation state of Co in CoO_x during the NO reduction by CO reaction. The important factor, as hypothesized above, a possible correlation with its catalytic activity, is not yet fully understood. The main reason is the challenge of carrying out such investigation in realistic working conditions and the difficulty in correlating the changes that occur in this multicomponent system (catalyst, support, reactants, inter-mediates, and products) to identify the active species in the catalytic process.

Herein, we report a systematic study of a series of CeO_2-supported CoO_x catalysts by a multimodal approach, involving in situ synchrotron X-ray absorption spectroscopy (XAS), in situ diffuse reflectance infrared Fourier transform spectroscopy (DRIFTS), and other complementary techniques (e.g., Raman spectroscopy, X-ray diffraction (XRD), and Brunauer−Emmett−Teller (BET) surface area analysis in addition to catalytic activity and product selectivity measurement). In this work, by comparing the results of different techniques, the following fundamental questions were addressed to understand the NO reduction by CO over CeO_2-supported CoO_x catalysts.

- What is the monolayer coverage of CoO_x/CeO_2 catalysts?
- How are the molecular and electronic structures of samples affected by Co surface density?
- How are the molar reaction rates affected by Co loadings?
- What are the key parameters to control the NO reduction by CO reaction?
- What are the intermediate species and possible reaction mechanisms of NO reduction by CO reaction with CoO_x/CeO_2 catalysts?

2. EXPERIMENTAL SECTION

2.1. Catalyst Synthesis. The supported cobalt oxide (CoO_x) was prepared by the incipient wetness impregnation of an aqueous solution with varying concentrations of cobalt(II) nitrate hexahydrate ($Co(NO_3)_2 \cdot 6H_2O$, ACS grade, 98.0–102.0%, crystalline, Alfa Aesar) onto CeO_2 (Rhodia, HSA 5). After impregnation, the samples were dried at room temperature (RT) for 12 h. The initially dried samples were transferred to a tube furnace (Lindberg/Blue Mini-Mite Tube Furnace, model TF55030A-1) and further dried in air (dry grade, from Airgas) at 120 °C (2 °C/min ramping rate) for 12 h and subsequently calcined at 400 °C (5 °C/min ramping rate) for 6 h. After the calcination process, the samples were sieved through a 40-mesh sieve (Fisherbrand).

2.2. Specific Surface Area and Pore Volume Measurement. The specific surface area and pore volume of the series of CoO_x/CeO_2 catalysts were calculated from N_2 adsorption/desorption isotherms using the Brunauer–Emmett–Teller (BET) theory and the Barrett–Joyner–Halenda methods, respectively. The Micromeritics ASAP 2010 device was used at the liquid N_2 temperature of −196 °C for analysis. Before the analysis, 0.1 g of catalyst was pretreated in a vacuum at 300 °C for 4 h to remove impurities.

2.3. Inductively Coupled Plasma Atomic Emission Spectrometry (ICP-AES). The Co element content in the series of CoO_x/CeO_2 catalyst was determined by the ICP-AES method. The ICP-AES experiment was carried out with an iCAP 6000 Series ICP-OES spectrometer (Thermo Fisher Scientific) accompanied by an ASX-260 Autosampler (CETAC). The samples were dissolved in nitric acid before testing. A cobalt standard (1000 mg/L Co in 2% nitric acid, from Sigma-Aldrich) was used as the reference.

2.4. Raman Spectroscopy. The molecular structure and bond vibration of CoO_x/CeO_2 samples were determined via Raman spectroscopy. For comparison, bulk Co_3O_4, CoO, and CeO_2 Raman spectra were also collected. Raman spectra were recorded with visible (514 nm, He–Ne laser) excitation (Renishaw, inVia Raman microscope) under the ambient atmosphere. The scattered photons were directed into a single monochromator and focused onto an air-cooled charge-coupled device. The Raman shift was calibrated with a built-in silicon standard sample. The spectral acquisition times were 10 scans accumulated with 10 s/scan.

2.5. Powder X-ray Diffraction. To determine the crystalline phases in the catalysts, powder X-ray diffraction patterns were obtained with a Rigaku (mode 1 SmartLab) diffractometer with Cu Kα radiation (λ = 0.1542 nm). The voltage and current of X-ray were 40 kV and 30 mA, respectively. The patterns were collected at a scanning step size of 0.02° at a rate of 2.5°/min and in a 2θ range from 20 to 70°.

2.6. X-ray Absorption Spectroscopy (XAS). In situ XAS measurements were performed at beamline BL 2-2 at the Stanford Synchrotron Radiation Lightsource, SLAC National Accelerator Laboratory, and at the Inner-Shell Spectroscopy (ISS) beamline at National Synchrotron Light Source II, Brookhaven National Laboratory. The Co K edge data were collected in the fluorescence mode. To compare the structures of the as-prepared samples with different Co weight loadings, ex situ XAS measurements were performed. For these measurements, the sample powders were spread onto an adhesive tape, then folded several times and mounted onto the sample holder. To investigate the structure evolution of Co

during the NO reduction by CO reaction, XAS data were also collected in the in situ conditions. For in situ measurements, the sample powder was loaded into the Clausen plug-flow reaction cell,[56] consisting of a quartz tube with 0.9 mm inner diameter and 1.0 mm outer diameter. The treatments on the sample were: helium at RT → helium at 400 °C → gas mixture of CO, NO, and He (CO/NO = 1:1) at 400 °C → keep gas mixture flowing while decreasing temperature to RT by the step of 100 °C. At each target temperature, up to six consecutive scans were collected to improve the signal-to-noise ratio.

2.7. Catalytic Activity Tests. The gas phase reactions were carried out in a fixed bed quartz reactor (7 mm inner diameter, 9.6 mm outer diameter, and 9.6 inches long) packed with sieved catalyst powder and quartz wool. Catalyst loadings were ~40 mg. Flow rates were measured by mass flow meters (FMA-1700A series, from Omega Engineering, Inc.) and the temperature was monitored by a K-type thermocouple (Omega). Reaction products were identified and analyzed by Fourier transform infrared (FT-IR, PerkinElmer, Frontier) with a gas cell (MARS series model #MARS 0.4L/3V-SS, International Crystal Laboratories). For the NO reduction by CO reaction, 500 ppm NO (2000 ppm with helium balance, Airgas) and 500 ppm CO (2000 ppm with helium balance, Airgas) were used in the reactions with argon (UHP Grade, Airgas) balance. The total flow rate was 200 mL/min in all experiments and the reaction was allowed to proceed for at least 30 min at each reaction temperature before the data collection. The blank tests indicated that the conversions of NO and CO were negligible without the catalyst. The NO and CO conversions were calculated according to the following equations

$$\text{NO conversion} = \frac{(\text{NO})_{\text{inlet}} - (\text{NO})_{\text{outlet}}}{(\text{NO})_{\text{inlet}}} \times 100\% \tag{1}$$

$$\text{CO conversion} = \frac{(\text{CO})_{\text{inlet}} - (\text{CO})_{\text{outlet}}}{(\text{CO})_{\text{inlet}}} \times 100\% \tag{2}$$

2.8. In Situ Diffuse Reflectance Infrared Fourier Transform Spectroscopy (in Situ DRIFTS). The in situ DRIFTS experiments were carried out with Thermo Scientific Nicolet iS10 FT-IR and a Harrick Praying Mantis chamber. The catalyst sample was first pretreated at 400 °C in flowing Ar (20 mL/min) for 30 min. After pretreatment, the sample was cooled to room temperature under flowing Ar and a background spectrum was taken. For the NO + CO reaction, a mixture of 5% CO, 5% NO, and balance He was used at a flow rate of 20 mL/min. Before the collection of a spectrum, the reaction was allowed to proceed for 20 min at each temperature (25, 50–400 °C with a 50 °C increase). Each spectrum was recorded at 4 cm^{-1} resolution and was the average of 32 scans.

3. RESULTS

3.1. Specific Surface Area and Surface Density. BET results for the series of CoO_x/CeO_2 catalyst samples are shown in Table 1. The actual Co wt % of the samples were also confirmed by the ICP-AES test and the results are included in Table 1 as well. It was observed that the specific surface area and pore volume of the samples decrease with increasing Co loading. For instance, the as-received supporting material CeO_2 had the highest surface area of 235 m^2/g, whereas the 30

Table 1. BET Results, Surface Densities, Pore Volumes and ICP-AES Results of CoO$_x$/CeO$_2$ Catalysts of Various Co Loadings

Co wt % by calculation	Co wt % by ICP-AES	surface area per unit mass (m^2/g)	surface density (Co/nm^2)	pore volume (cm^3/g)
0		235	0	0.17
0.5	0.5	212	0.2	0.17
2	2.1	191	1.1	0.15
4	3.8	180	2.3	0.14
6	6.1	173	3.5	0.14
8	8.0	158	5.2	0.13
10	10.5	143	7.1	0.12
20	21.7	113	18.1	0.11
30	29.1	98	31.3	0.10

wt % sample (98 m^2/g) showed the lowest surface area of all of the prepared CoO$_x$/CeO$_2$ samples. Compared to the as-received CeO$_2$, the specific surface area of the 30 wt % CoO$_x$/CeO$_2$ sample was decreased by 58%. The cobalt oxide surface density (Co/nm^2) of the CoO$_x$/CeO$_2$ catalyst samples was calculated using the sample surface area

$$\text{surface density of Co} = \frac{\frac{W_{Co}/100}{M_{Co}} \times N_A}{S} \qquad (3)$$

where W_{Co} is the weight percentage of Co, M_{Co} is the atomic weight of Co, N_A is the Avogadro number, and S is the sample surface area.

The N$_2$ adsorption/desorption isotherm results and the pore size distribution of the selected catalysts are shown in Figure 1. From the results, the tested CoO$_x$/CeO$_2$ catalyst samples showed type IV isotherm, which was typical for mesoporous materials (Figure 1a).[57] The sharp steps of $P/P^0 = 0.4-0.8$ can be ascribed to the capillary condensation within the uniform ceria mesoporous structure.[58,59] It can also be observed from Figure 1a that as the Co loading increased, a decrease in the absorbed volume was noticed, which corresponded to the decrease in the BET surface area and pore volume. The pore size distribution of the samples showed that the average pore diameter of all of the tested CoO$_x$/CeO$_2$ samples was around 3.5 nm and did not change as the Co loading increased (Figure 1b). As shown in the results from Table 1 and Figure 1, a decrease in the specific surface area and pore volume indicated closure of some of the ceria pores by impregnation of cobalt on the surface.
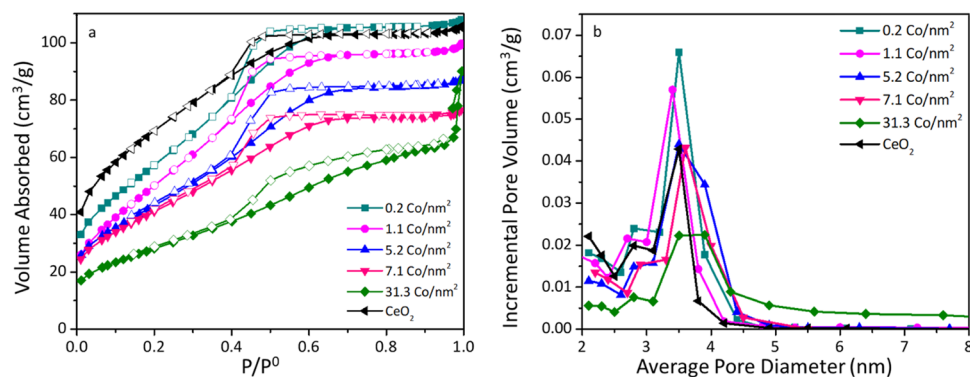
3.2. Powder X-ray Diffraction. The powder X-ray diffraction (XRD) technique was used to detect the crystalline structures on the surface of the as-prepared CoO$_x$/CeO$_2$ catalyst samples as well as bulk CeO$_2$ and synthesized bulk Co$_3$O$_4$ for comparison. As shown in Figure 2, only Co$_3$O$_4$ and
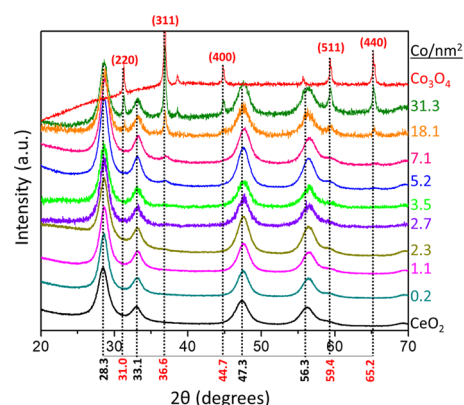
Figure 2. XRD patterns for CoO$_x$/CeO$_2$ catalysts of various Co surface densities. The values of the surface density (their correspondence to the Co loading is in Table 1) are shown on the right.

CeO$_2$ phases in the prepared catalysts were detected. The prominent peaks from fluorite CeO$_2$ (face-centered cubic structure, PDF# 97-002-8709) included 28.3, 33.1, 47.3, and 56.3°, representing (111), (200), (220), and (311) reflections, respectively. For comparison, the XRD pattern of the as-prepared bulk Co$_3$O$_4$ sample was also included and was similar to the pattern of spinel Co$_3$O$_4$ (PDF# 97-006-9369). The spinel Co$_3$O$_4$ structure had (220), (311), (400), (511), and (440) reflections at 31.0, 36.6, 44.7, 59.4, and 65.2°, respectively.

For the CoO$_x$/CeO$_2$ catalyst samples, there were no obvious Co$_3$O$_4$ patterns at 36.6° under the 5.2 Co/nm^2 surface density sample. Starting from the 5.2 Co/nm^2 sample, the 36.6° peak from spinel Co$_3$O$_4$ became detectable. With the increased Co surface density, the 36.6° peak intensity also increased, indicating the formation of larger crystalline Co$_3$O$_4$ structures on the surface of CeO$_2$. Other characteristic weak peaks of spinel Co$_3$O$_4$ did not show up until the Co surface density reached 18.1 Co/nm^2. Meanwhile, the prominent fluorite CeO$_2$ patterns could be found in all of the as-prepared CoO$_x$/CeO$_2$ samples, and no shift was observed in the samples' XRD

Figure 1. (a) N$_2$ adsorption (close symbol)/desorption (open symbol) isotherms of selected CoO$_x$/CeO$_2$ samples. (b) Pore size distributions of selected CoO$_x$/CeO$_2$ samples. P^0 =1 atm.

patterns compared to pure CeO_2. This result suggests that, for all of the as-prepared CoO_x/CeO_2 samples, ranging in surface density from 0.2 to 31.3 Co/nm^2, impregnated Co was not substituted for Ce^{4+} in the CeO_2 structure or a solid solution (e.g., $Co_xCe_{1-x}O_2$) material was not formed.[60] It is reasonable to conclude that CeO_2 was stable and retained its crystalline structure (no structural changes in the fluorite CeO_2 lattices), whereas the precursor $Co(NO_3)_2$ converted to CoO_x and Co_3O_4 with CeO_2 interaction after calcination.

3.3. Raman Spectroscopy. The Raman spectroscopy technique has been extensively used for identifying the molecular structure of supported metal oxide catalysts and nanosized crystal formation of surface metal oxide.[27,61,62] Raman spectra of all of the prepared samples, including pure CeO_2, calcined $Co(NO_3)_2$ (denoted as Co_3O_4), and bulk CoO, are shown in Figure 3. The Raman spectra showed that
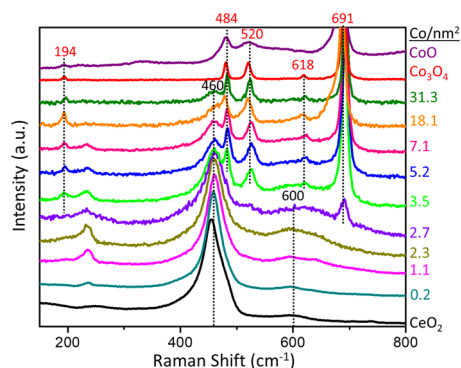

Figure 3. Raman spectra of CoO_x/CeO_2 catalysts of various Co surface densities. The values of the surface density (their correspondence to the Co loading is in Table 1) are shown on the right.

up to 2.3 Co/nm^2 surface density samples, the broad and strong bands at 460 cm^{-1} are dominant. The 460 cm^{-1} band is widely accepted as the symmetrical stretching of the Ce−O bond in F_{2g} vibration of fluorite CeO_2.[63,64] Also, there was another weak and broad band at ~600 cm^{-1}, which could be assigned to the D-band vibration of CeO_2.[65] The D-band vibration of CeO_2 is believed to be associated with Frenkel defects and oxygen vacancies due to the presence of Ce^{3+} ions in the CeO_2 lattice.[66]

Starting from the 2.7 Co/nm^2 catalyst sample, a band at ~691 cm^{-1} was observed in the Raman spectra and this peak

could be assigned to the A_{1g} vibration in Co_3O_4. Other weaker bands around 194 cm^{-1} (weak, F_{2g}-mode), 484 cm^{-1} (medium, E_g-phonon mode), 520 cm^{-1} (medium, F_{2g}-mode), and 618 cm^{-1} (weak, F_{2g}-mode) were also noticed to appear from 3.5 Co/nm^2.[67] Although these bands were also observed in the CoO spectrum, all peaks were much broader than those in the Co_3O_4 spectrum. It is worthwhile to note that the Co_3O_4 crystalline peak was not clearly detected until 3.5 Co/nm^2 in XRD spectra (Figure 2). This difference between the Raman and XRD results indicated that the Co_3O_4 nanocrystalline structure was already formed in the 2.7 Co/nm^2 sample, but the crystalline size might not be large enough to be detected by powder XRD. Based on the Raman spectroscopy results, the monolayer coverage of the prepared CoO_x/CeO_2 is expected to be between 2.3 and 2.7 Co/nm^2. Although both XRD and Raman spectroscopy provided information on monolayer coverage and crystalline structure formations of surface species, the electronic structure of surface species (e.g., the oxidation state of Co) was not clearly identified. Changes of Co oxidation states under ex situ and in situ conditions were investigated by X-ray absorption spectroscopy (XAS) and reported below (Section 3.4).

3.4. X-ray Absorption Spectroscopy. To unveil the oxidation state−activity relationship, ex situ and in situ XAS experiments were performed. Multiple measurements were carried out to investigate the oxidation state of Co species in CoO_x/CeO_2 catalysts with different Co loadings, under reaction conditions, and compared between fresh and used samples (e.g., 7.1 Co/nm^2). As shown in Figure 4a, the XANES spectra of samples with low surface density (0.2 Co/nm^2 and 1.1 Co/nm^2 samples) are quite unique, having features different from those of CoO and Co_3O_4. But for these two samples, the edge region of XANES spectra is resembling that of CoO, suggesting that in these two samples Co is most likely in the 2+ state. With the increase of the surface density, the XANES spectra transform to resemble that of Co_3O_4. Comparing with the activity test results in the following section, XANES result suggested that Co with a higher oxidation state could be the reason for the higher catalytic activity. Figure 4b showed XANES result of the used 7.1 Co/nm^2 sample in comparison with the fresh 7.1 Co/nm^2 sample. The used sample showed a significantly different spectrum from that of the fresh sample, indicating that the oxidation state of Co species underwent a partial transformation from the Co_3O_4-like state to the CoO-like state after the reaction. The
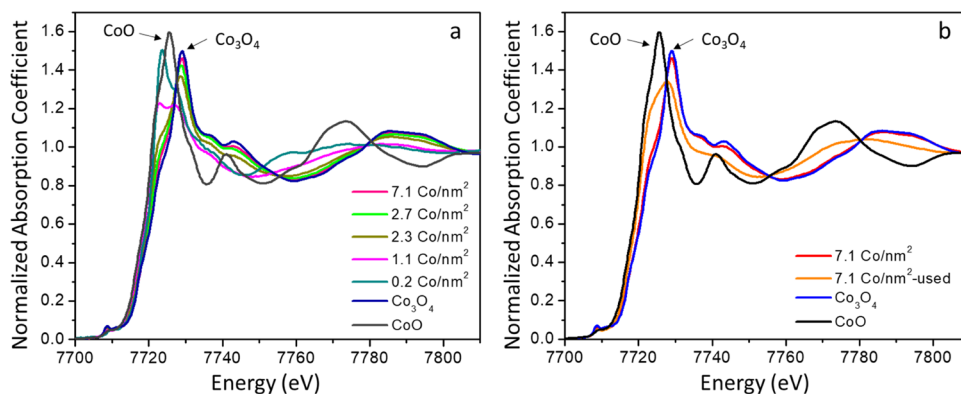

Figure 4. Normalized Co K edge XANES spectra of (a) a series of CoO_x/CeO_2 samples and (b) fresh and used 7.1 Co/nm^2 CoO_x/CeO_2 samples taken ex situ at room temperature. The XANES spectra of CoO and Co_3O_4 were also included for comparison.
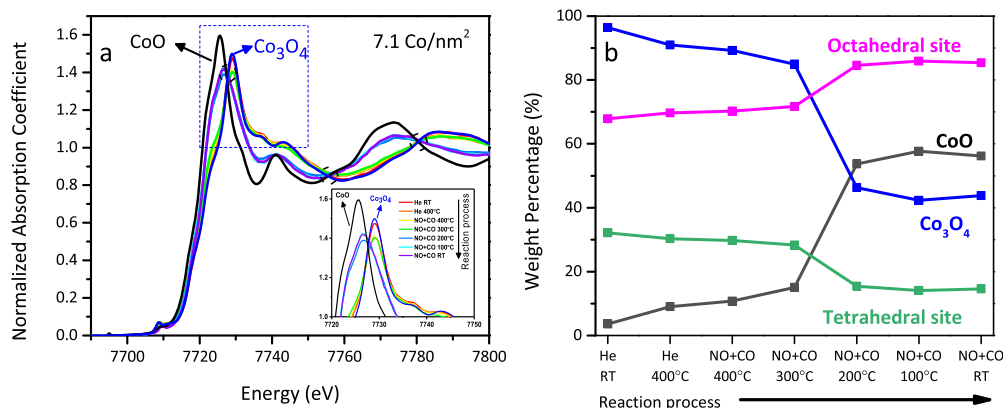
Figure 5. (a) Normalized Co K edge XANES spectra of the 7.1 Co/nm^2 sample under different conditions. For comparison, the energy spectra of CoO and Co_3O_4 were also included. Inset: rectangle section to highlight the 1.0−1.7 normalized absorption coefficient and 7720−7750 eV regions. (b) The weight percentage change of Co_3O_4/CoO and Co octahedral/tetrahedral sites under different conditions.
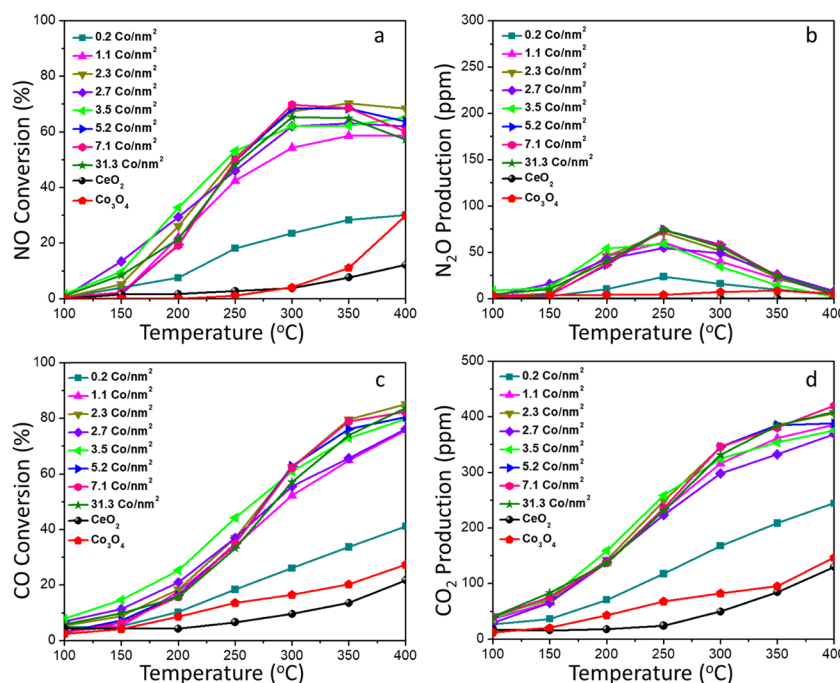

Figure 6. Catalytic activity results for NO reduction by CO reaction over CoO_x/CeO_2 catalysts. (a) NO conversion under different temperature conditions, (b) N_2O production under different temperature conditions, (c) CO conversion under different temperature conditions, (d) CO_2 production under different temperature conditions. Reaction conditions: 50 mL/min (500 ppm) NO, 50 mL/min (500 ppm) CO balanced with argon, total flow rate 200 mL/min. ∼40 mg of sample was used.

activity and XANES results clearly explained that the oxidation state of Co played an important role in governing the NO reduction by CO reaction and was directly related to the catalyst deactivation.

Figure 5 showed the result of in situ XANES during the NO reduction by CO using the 7.1 Co/nm^2 sample at different temperatures. Helium (He) gas at RT → He gas at 400 °C → NO + CO at 400 °C → 300 °C to 100 °C → NO + CO at RT. As shown in Figure 5a, the XANES spectra under helium at RT and 400 °C, and those under reacting gases (NO + CO) at 400 and 300 °C were very similar and almost identical to that of Co_3O_4. When the temperature decreased to 200 °C and below 200 °C, the spectra changed and became more similar to that of CoO. The presence of several isosbestic points, marked by dashed-circles in Figure 5a, indicated that the sample transformed directly from one phase to another. Furthermore,

because the spectra for bulk Co_3O_4 and CoO oxides showed the same isosbestic points, it could also be concluded that the catalyst structure changed within the range of structures from pure Co_3O_4 and CoO. The linear combination analysis was then used to determine the concentrations of Co_3O_4 (starting phase) and CoO (final phase) at different temperatures. The fitting range was 7698−7778 eV and the obtained results are plotted in Figure 5b. The result of linear combination fitting revealed that the fraction of Co_3O_4 (or CoO) in the sample dramatically decreased (or increased) when the temperature dropped below 300 °C. In addition to the Co oxidation state, the coordination of CoO_x (CoO or Co_3O_4) was also considered. Co^{2+} ions were mainly in octahedral interstices in CoO. In Co_3O_4, however, Co^{2+} ions were in tetrahedral interstices and Co^{3+} were in octahedral interstices, respectively, and the ratio of Co^{2+} to Co^{3+} in Co_3O_4 was 1:2.[74,75] The

changes are plotted in Figure 5b as well. When combined with the result of the catalytic performance of this catalyst, this trend again supported the hypothesis that the reduction of Co to the 2+ state might be the reason for the lowered NO and CO conversion.

3.5. Catalytic Activity. The relationship between the molecular structure and catalytic activity of CoO_x/CeO_2 catalysts was investigated for the reduction of NO by CO. The Co loading and temperature dependences of NO conversion, CO conversion, N_2O production, and CO_2 production are shown in Figure 6. The main reaction products were N_2O, N_2, and CO_2. Note that no NO_2 production under the conditions of this experiment was observed. As shown in Figure 6a,c, bulk CeO_2 and bulk Co_3O_4 showed very low NO and CO conversion. In the case of very low Co loading samples, such as 0.2 Co/nm^2, catalytic activity was improved compared to CeO_2 and Co_3O_4, whereas maximum NO and CO conversion were still <20 and <40%, respectively. When Co loading was higher than 0.2 Co/nm^2, both NO and CO conversion increased significantly, especially at ≥250 °C. NO conversion over 1.1−31.3 Co/nm^2 catalysts increased up to 300 °C and then leveled off or decreased at >300 °C. Although ≥2.7 Co/nm^2 samples already contain the crystalline Co_3O_4 structure (Figure 3), it did not decrease NO conversion.

Interestingly, for all of the CoO_x/CeO_2 catalyst samples, the production of N_2O depended highly on the reaction temperatures (Figure 6b). N_2O concentrations increased continuously with increased reaction temperature up to 250 °C and then decreased at higher temperatures (>250 °C). This result indicated that at >250 °C, the catalyst became very active for N_2O decomposition into N_2, thus led to the decrease in N_2O production. These results corresponded to the well-accepted two-step reaction process

$$2NO + CO \rightarrow N_2O + CO_2 \tag{4}$$

$$N_2O + CO \rightarrow N_2 + CO_2 \tag{5}$$
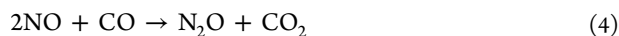
The observed N_2O formation−decomposition as a function of reaction temperature was matched well to previous studies. Xue et al.,[55] reported that less than 10% N_2O was consumed at 150 °C using the Co_3O_4/CeO_2 catalyst, whereas ~40% N_2O was reduced at 200 °C. Liotta et al.,[29] also reported that for CoO_x/CeO_2 catalysts, 50% of the N_2O was converted at ~ 250 °C and 100% of the N_2O was converted at ~300 °C. At very high reaction temperatures, 700−850 °C, Iwanek et al.,[68] reported that N_2O decomposition over a series of CoO_x/CeO_2 catalysts increased with increasing reaction temperature.

Figure 6c,d shows that CO conversion increased monotonically with increased reaction temperature, and all the consumed CO was converted to CO_2 by NO (eq 4) and N_2O (eq 5). Compared to NO conversion, CO conversion was lower (or similar) at ≤300 °C and higher at >300 °C. This result, especially ≤300 °C, agrees with the findings from the literature over supported Pd catalysts. Cónsul et al.,[69] tested Al_2O_3/SiO_2 supported Pd and Mo−Pd catalysts for the NO reduction by CO at 523−573K (250−300 °C) and claimed that the NO conversion was always higher than that of CO due to the N_2O formation. The authors also observed higher N_2O selectivity than that of N_2 which is different from our results at 300 °C. As shown in Figure S1, at ≥300 °C, N_2 selectivity over the series of CoO_x/CeO_2 catalysts was much higher than that of N_2O. Therefore, the N_2O selectivity does not always follow the NO conversion ratio although it is closely related to the

reaction temperatures. From the results so far, it can be concluded that: (1) The NO conversion with varied Co loadings follows the trend: 2.3−31.3 Co/nm^2 (monolayer and over-monolayer) > 1.1 Co/nm^2 (sub-monolayer) ≫ 0.2 Co/nm^2 (very low Co concentration) ≫ bulk Co_3O_4 > bulk CeO_2; (2) for most CoO_x/CeO_2 catalysts, NO conversion increased with increased reaction temperature up to 300 °C; (3) at lower temperature (up to 250 °C), N_2O formation is favorable, whereas at higher temperature (>250 °C), N_2 formation is favorable.

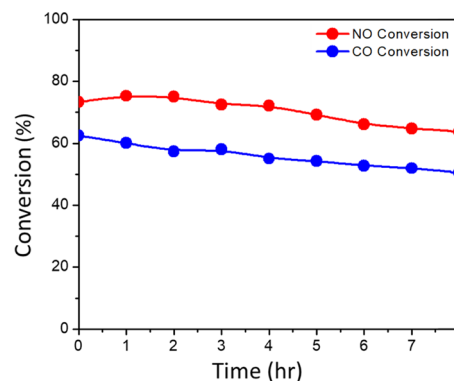To investigate the stability of the catalyst, the 7.1 Co/nm^2 sample was used for the time-on-stream test. Figure 7

Figure 7. Time-on-stream results for NO reduction by CO reaction at 300 °C over the 7.1 Co/nm^2 CoO_x/CeO_2 catalyst. Reaction conditions: 50 mL/min (500 ppm) NO, 50 mL/min (500 ppm) CO balanced with argon, total flow rate 200 mL/min. ~40 mg of sample was used.

illustrates that NO and CO conversions decreased slightly after reacting under 300 °C for 8 h. It is speculated that the decreased NO and CO conversion could be ascribed to the changes of the molecular or electronic structure of the catalyst. Figure S2 showed the Raman spectra of the 7.1 Co/nm^2 sample before and after the reaction. Compared to the fresh sample's spectrum, the used sample also contained a band at 460, 484, 520, and 691 cm^{-1}, but with changed peak intensities. Specifically, the used sample's Raman peak intensity ratio of $I_{460cm^{-1}}/I_{691cm^{-1}}$ increased compared to the fresh sample. It was also observed that the peak intensity and broadness of the band around 520 and 618 cm^{-1} of the used sample were very similar to the CoO spectrum. From the Raman spectra, it can be concluded that both molecular and electronic structures of the catalyst changed after the reaction. From previous literature, catalyst deactivation could be caused by the change of the Co oxidation state and deposition of carbonate species.[41,70−72] Because most reaction temperatures in this work were higher than that of carbonate desorption (~100 °C),[73] it could be ruled out in the current work.

3.6. In Situ Diffuse Reflectance Infrared Fourier Transform Spectroscopy (in Situ DRIFTS). In situ DRIFTS was used to provide an insight into the intermediate species during the NO reduction by CO reaction and possible reaction mechanisms. Figure 8 shows the adsorption spectra during the NO reduction by CO on the 2.7 Co/nm^2 sample as a function of reaction temperatures (25−400 °C). Several surface species' bands due to NO and CO adsorption can be observed. In Figure 8a, IR bands were observed at 844 cm^{-1} (from CO adsorption[76]), 1013 cm^{-1}, and 1612 cm^{-1} (O−N−O symmetric vibration in the bridging bidentate nitrate
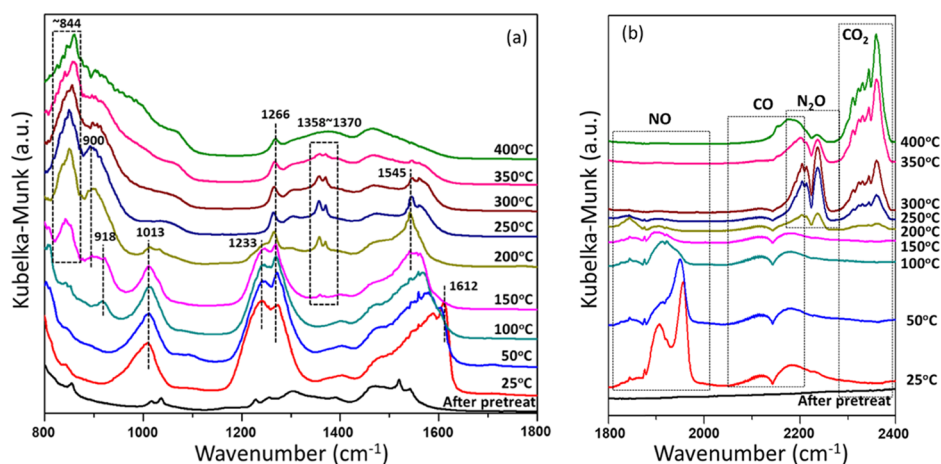
Figure 8. In situ DRIFTS spectra of the 2.7 Co/nm^2 sample. (a) 800−1800 cm^{-1} region and (b) 1800−2400 cm^{-1} region. Reaction conditions: 10 mL/min (5% CO in He balance) and 10 mL/min (5% NO in He balance), total flow rate, 20 mL/min. ~50 mg of samples were used. For "after pretreat", the conditions were in Ar atmosphere and at room temperature.

structure[44]), 1233 cm^{-1} (O−N−O asymmetrical vibration in the linear nitrite structure[77]), 1545 cm^{-1} (bridging monodentate nitrate[78]), 1266 cm^{-1} bands (monodentate nitrate[79]), and 1358−1370 cm^{-1} (carboxylates[80,81]). Upon taking a closer look, it can be noticed that most nitrate (1013 and 1612 cm^{-1}) and nitrite (1233 cm^{-1}) species formed at lower than 250 °C and then disappeared at higher temperature conditions (>250 °C). In addition to the nitrate and nitrite bands, from 150 °C, carboxylate bands (1358−1370 cm^{-1}) were observed and disappeared at 400 °C. It can be hypothesized that at lower temperature (≤150 °C), CO adsorption was not preferred due to the lack of oxygen vacancies. At higher temperature conditions, as the adsorbed NO started to decompose, they could possibly produce more oxygen vacancies on CeO$_2$ and facilitate more space for CO adsorption which formed carboxylates. The surface nitrates and nitrites, and carboxylate bands were also observed on the bulk CeO$_2$ spectra (Figure S3a), but these bands still existed even at 300 and 400 °C, respectively. The results clearly show that the supported CoO$_x$ catalyst improved the ability for desorption and dissociation of intermediate species at lower temperatures.

In addition to the surface intermediate species, the change of band intensities of gas components is also shown in Figure 8b. The intensity of both NO and CO bands decreased with increasing reaction temperature. The N$_2$O band intensity at 2150−2250 cm^{-1} increased with increasing temperature up to 250−300 °C and then gradually decreased as we further increased the reaction temperature. The N$_2$O band almost disappeared at 400 °C and this also corresponded to our findings in the activity test (Figure 6b), where we found that N$_2$O production increased up to 250 °C, then decreased to almost none at 400 °C. In the case of CO$_2$, the band intensity continuously increased up to 400 °C, also agreeing with our previous findings (Figure 6d). From the activity results (Figure 6a,c), bulk CeO$_2$ showed very low catalytic activity for NO and CO conversion. In situ DRIFT spectra of CeO$_2$ (Figure S3b) also supported the activity results. The bands of NO and CO were observed up to 400 °C and peak intensities did not change much from 50 to 400 °C. N$_2$O and CO$_2$ bands in bulk CeO$_2$ spectra were observed at a much higher temperature (300 °C) than that of CoO$_x$/CeO$_2$ (200 °C). The band intensity of N$_2$O in bulk CeO$_2$ spectra was also much lower than that of CoO$_x$/CeO$_2$. The observed in situ DRIFT results

confirmed the critical role of surface CoO$_x$ and showed that surface CoO$_x$ facilitated N$_2$O decomposition at a lower temperature compared to bulk CeO$_2$.

In the case of bulk Co$_3$O$_4$, it can be noticed that there were barely any surface intermediate species during the NO reduction by CO, except for the bidentate nitrate at 1612 cm^{-1} (Figure S4a), which disappeared after 100 °C, this is also in accordance with bulk CeO$_2$ and the 2.7 Co/nm^2 sample. The difference amount of intermediate species on Co$_3$O$_4$ and other tested samples was possibly because Co$_3$O$_4$ is not a porous material like CeO$_2$, resulting in less positions/vacancies for gas adsorption. The bands of NO and CO were observed up to 400 °C and peak intensity decreased slowly with increasing reaction temperature. N$_2$O and CO$_2$ bands in bulk Co$_3$O$_4$ spectra were observed from 200 °C which are similar to that of CoO$_x$/CeO$_2$. The band intensity of N$_2$O and CO$_2$ in bulk Co$_3$O$_4$ was much higher than that of bulk CeO$_2$ and this result matched the concentration results in Figure 6b,d.

4. DISCUSSION

The molecular and electronic structure−catalytic activity relationship over a series of CoO$_x$/CeO$_2$ catalysts has been investigated using both conventional (e.g., XRD and Raman) and advanced spectroscopic techniques (e.g., in situ XAS). Specifically, the comparison among all results obtained for samples with different Co weight loadings from 0.2 to 31.3 Co/nm^2, the fresh and used catalysts of 7.1 Co/nm^2, as well as the temperature-dependent data from 100 to 400 °C, revealed one common property for all investigated conditions, that is, the catalysts with a higher Co oxidation state (+3) have higher catalytic activity in the NO reduction by CO reaction.

With ex situ Raman and XANES, we were able to identify the molecular structure and the Co oxidation state (e.g., +2 and +2/+3) in CoO$_x$/CeO$_2$ catalysts with different Co loadings. In both Raman and XANES results, the structure of Co$_3$O$_4$ was clearly observed starting from the 2.3−2.7 Co/nm^2 sample (Figures 3 and 4a), which corresponded to the activity results. Moreover, in the case of the 1.1 Co/nm^2 sample, the XANES spectrum showed an intermediate state between CoO and Co$_3$O$_4$, which explained its slightly lower activity results than other samples from 2.3 to 31.3 Co/nm^2. It is worthwhile to highlight that the XANES provided more precise information on monolayer coverage in this series of

CoO_x/CeO_2 catalysts than Raman spectroscopy or XRD result. XAS showed the strong feature of Co_3O_4 crystal formation in the 2.3 Co/nm^2 sample (Figure 4a), whereas Raman spectroscopy results showed that the monolayer coverage for CoO_x/CeO_2 is in between 2.3 and 2.7 Co/nm^2 (Figure 3). Recently, Peck et al.[27] collected data from literature studies for the surface density values of Co_3O_4 formation in the CoO_x/CeO_2 catalysts and reported the onset of monolayer formation using the XRD, Raman, and XPS. The authors concluded that the Raman spectroscopy results are in good agreement with the XPS (surface sensitive technique) data, and the monolayer coverage is just below 2.58 Co/nm^2, which matches well with our Raman data. Although the inhomogeneity of the surface (CoO_x) on ceria support cannot be completely ignored, and Co_3O_4 microcrystalline formation under the sub-monolayer coverage may also exist, it is reasonable to say that XAS showed a higher sensitivity in detecting the Co_3O_4 microcrystals than other spectroscopic techniques used in this work.

Moreover, samples with ≥2.3 Co/nm^2 surface density showed significantly higher NO and CO conversions in the NO reduction by CO reaction compared to the lower Co density samples, bulk CeO_2, and bulk Co_3O_4 (Figure 6). To understand the inherent activity of CoO_x/CeO_2, molar rates of the reaction (moles of NO converted by each mole of Co in unit time) were calculated at 150 °C where NO conversion is <20% to satisfy the differential reactor conditions.

As shown in Figure 9, the molar rate increases monotonically with increasing Co surface density and then decreases at
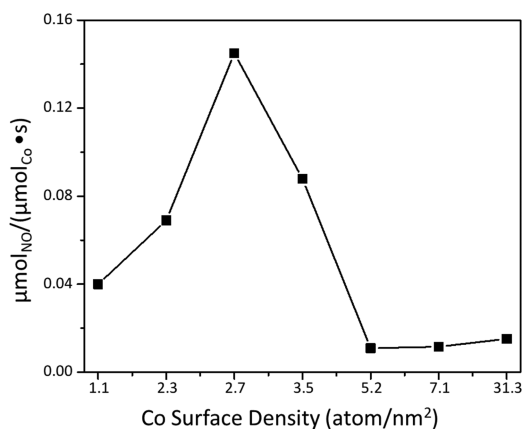

Figure 9. Molar rate in the NO reduction by CO reaction with CoO_x/CeO_2 catalysts at 150 °C.

higher than 2.7 Co/nm^2 samples. As shown in the Raman and XANES results (Figures 3 and 4), the samples with the surface density between 2.3 and 2.7 Co/nm^2 were believed to have monolayer coverage of CoO_x. Based on the molar rate and spectroscopy results, it is speculated that increasing the number of Co−O−Ce linkages (or higher dispersion of CoO_x) and the small size of the Co_3O_4 crystalline structure can improve the inherent catalytic activity due to the electronic metal support interaction.[27] However, further increase of the Co content (≥3.5 Co/nm^2), which forms a large size of the crystalline Co_3O_4 structure, will lead to a decreased catalytic activity.

By comparing the N_2O formation with different Co loading samples as a function of reaction temperature, it was observed that N_2O formation had similar trends, although absolute values depended on the Co surface density, that is, N_2O

production increased up to 250 °C and then decreased at higher temperatures (>250 °C) as shown in Figure 6b. Deng et al.[19,82] investigated the catalytic performance for the NO reduction by CO reaction over a series of $Ce_{20}M_1O_x$ (M = Zr, Cr, Mn, Fe, Co, Sn; Ce/M molar ratio = 20:1) composite oxides and Cu supported on composite catalysts. Although the authors used different catalyst synthesis methods and co-precipitation methods, N_2O (or N_2) selectivity result matched well with our N_2O formation trend and the highest N_2O (or lowest N_2) selectivity was obtained at 200 °C. Based on the in situ DRIFT spectroscopy data, it was observed that at lower temperature (<275 °C) nitrite (NO_2^-)/nitrate (NO_3^-) species were formed on the catalyst surface and transformed to N_2O and N_2, whereas the adsorption of CO is limited. At higher temperature, ≥275 °C, CO adsorption increases which enhances the N_2O decomposition. From the literature results and the current study (Figures 6b and 8), it can therefore be concluded that NO to N_2 conversion is achieved through a two-step process during the NO reduction by CO: (1) NO converts to N_2O and (2) N_2O decomposes to N_2 over both supported and composite transition metal oxides.

In the case of the high Co loading sample, such as 7.1 Co/nm^2, the importance of Co oxidation state to NO and CO conversions during the reaction has been noted. Both conversion and in situ XANES results were taken into consideration here. The results of NO and CO conversions as a function of reaction temperature for the 7.1 Co/nm^2 sample were compared to the percentage of CoO and Co_3O_4 species on the catalyst surface calculated from in situ XANES (Figure 10). It is obvious that the Co_3O_4 percentage, NO
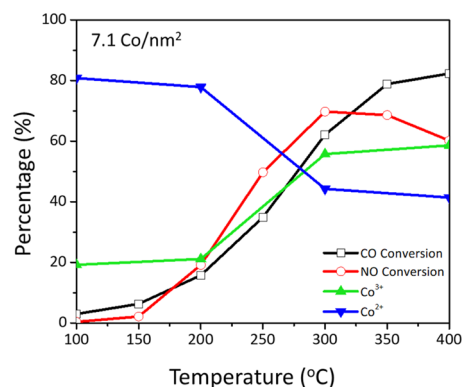

Figure 10. Relationship between surface species composition and NO reduction by CO reaction activities under different temperatures for the 7.1 Co/nm^2 sample.

conversion, and CO conversion all shared the same trend, suggesting that Co^{3+} sites should be the active sites in the CoO_x/CeO_2 catalyst. This finding proved that the oxidation state of Co species in the high loading CoO_x/CeO_2 sample plays an important role in the NO reduction by CO reaction.

By comparing the stability test results (Figure 7) and in situ XAS results (Figure 4b), we could reach similar conclusions as well. It shows that catalyst deactivation was closely related to the Co oxidation state. To be specific, the spectrum of the used sample was a mixture of Co_3O_4 and CoO phases, whereas the fresh 7.1 Co/nm^2 sample spectrum only had Co_3O_4 features. This finding again supported our speculation that during the NO reduction by CO reaction, as reaction time increased, the surface Co_3O_4 was gradually reduced to CoO by CO. The

reduction from Co_3O_4 to CoO was believed to be one of the reasons of the decrease of NO and CO conversions.

Comparing the current studies with the results from literature studies, the CoO_x/CeO_2 catalysts showed competitive NO and CO conversions, although precious metal catalysts (e.g., Pt and Pd) still showed higher activity during the NO reduction by CO reaction (Table S1). The use of supported CoO_x (or other transition metal oxide) catalysts for the NO reduction by CO was not investigated in this level of detail before. To the best of our knowledge, CeO_2 support showed higher NO and CO conversion compared to other supports like Al_2O_3, TiO_2, and ZrO_2. Although our finding helps in explaining the relationship between the activity and the structure/oxidation state of the CoO_x/CeO_2 catalysts, further studies of the metal−oxide support interaction will be required to not only understand but also control and, ideally, improve the catalytic activity of the CoO_x/CeO_2 catalyst and other transition metal oxides supported on ceria.

5. CONCLUSIONS

In this study, we have prepared a series of CoO_x/CeO_2 catalysts, investigated their catalytic activities and stabilities during the NO reduction by CO reaction, and explored the relationship between Co loading (0.2−31.3 Co/nm^2), Co oxidation state, and catalytic activities. The main conclusions in the work are:

(1) Using several spectroscopic techniques, we were able to identify the monolayer coverage of CoO_x/CeO_2 catalysts to be ~2.7 Co/nm^2.

(2) The surface structures of different Co loading samples were very different, from CoO-like structures in low Co loading samples to Co_3O_4-like structures in higher Co loading samples.

(3) Molar rates were also affected by the Co loadings of the CoO_x/CeO_2 catalysts, and we found that the molar rate of the 2.7 Co/nm^2 (around monolayer) sample was the highest among all of the prepared samples.

(4) We also identified the change of Co oxidation states during the reaction process and the higher Co oxidation state (+3) was more active than its lower counterpart (+2) in NO reduction by CO reaction. The oxidation states of surface Co species could play a very important role in determining the catalytic activity in NO reduction by CO reaction.

(5) Intermediate species (nitrates, nitrites, carboxylates, etc.) during the reaction process were noticed. A possible reaction mechanism was proposed, where under low temperatures (<250 °C), NO adsorption was favored over CO adsorption. The adsorbed NO can then form nitrates or nitrites and interact with each other or CO to produce N_2O, CO_2, and N_2. At higher temperatures, the oxidation state change of surface Co species created more oxygen vacancies on the catalyst surface, enabling nitrates/nitrites dissociation and CO adsorption. N_2 became the major product over N_2O at this temperature region also.

Overall, the obtained spectroscopic and activity results provided a way of investigating the molecular/electronic structure−activity relationship of a wide range of MO_x/CeO_2 (M−transition metal) catalysts.

■ ASSOCIATED CONTENT

ⓢ Supporting Information

The Supporting Information is available free of charge on the ACS Publications website at DOI: 10.1021/acs.jpcc.8b12442.

Comparison between catalysts found in the literature; Selectivity results in NO reduction by CO reaction; Raman spectra comparison of fresh and used 7.1 Co/nm^2 CoO_x/CeO_2 samples; DRIFTS spectra of bulk CeO_2; and DRIFTS spectra of bulk Co_3O_4 (PDF)

■ AUTHOR INFORMATION

Corresponding Author

*E-mail: taejin.kim@stonybrook.edu.

ORCID 🄭

Shuhao Zhang: 0000-0002-4240-3815
Anatoly I. Frenkel: 0000-0002-5451-1207
Taejin Kim: 0000-0002-0096-303X

Notes

The authors declare no competing financial interest.

■ REFERENCES

(1) Karemore, A. L.; Vaidya, P. D.; Sinha, R.; Chugh, P. On the Dry and Mixed Reforming of Methane over Ni/Al_2O_3—Influence of Reaction Variables on Syngas Production. *Int. J. Hydrogen Energy* **2016**, *41*, 22963−22975.

(2) Gandhi, H.; Graham, G.; McCabe, R. W. Automotive Exhaust Catalysis. *J. Catal.* **2003**, *216*, 433−442.

(3) Reihani, A.; Patterson, B.; Hoard, J.; Fisher, G. B.; Theis, J. R.; Lambert, C. K. Rapidly Pulsed Reductants for Diesel NO_x Reduction with Lean NO_x Traps: Comparison of Alkanes and Alkenes as the Reducing Agent. *J. Eng. Gas Turbines Power* **2017**, *139*, No. 102805.

(4) Held, W.; Koenig, A.; Richter, T.; Puppe, L. *Catalytic NO_x Reduction in Net Oxidizing Exhaust Gas*, 0148-7191; SAE Technical Paper; Society of Automotive Engineers, 1990.

(5) Okazaki, K.; Ando, T. NO_x Reduction Mechanism in Coal Combustion with Recycled CO_2. *Energy* **1997**, *22*, 207−215.

(6) Takeuchi, M.; Matsumoto, S. I. NO_x Storage-Reduction Catalysts for Gasoline Engines. *Top. Catal.* **2004**, *28*, 151−156.

(7) Shen, Y.; Ma, Y.; Zhu, S. Promotional Effect of Zirconium Additives on $Ti_{0.8}Ce_{0.2}O_2$ for Selective Catalytic Reduction of NO. *Catal. Sci. Technol.* **2012**, *2*, 589−599.

(8) Wang, X.; Shi, A.; Duan, Y.; Wang, J.; Shen, M. Catalytic Performance and Hydrothermal Durability of CeO_2−V_2O_5−ZrO_2/WO_3−TiO_2 Based NH_3-SCR Catalysts. *Catal. Sci. Technol.* **2012**, *2*, 1386−1395.

(9) Du, X.; Gao, X.; Hu, W.; Yu, J.; Luo, Z.; Cen, K. Catalyst Design Based on DFT Calculations: Metal Oxide Catalysts for Gas Phase NO Reduction. *J. Phys. Chem. C* **2014**, *118*, 13617−13622.

(10) Usberti, N.; Jablonska, M.; Di Blasi, M.; Forzatti, P.; Lietti, L.; Beretta, A. Design of a "High-Efficiency" NH₃-SCR Reactor for Stationary Applications. A Kinetic Study of NH₃ Oxidation and NH₃-SCR over V-Based Catalysts. *Appl. Catal., B* **2015**, *179*, 185−195.

(11) Ma, Z.; Wu, X.; Si, Z.; Weng, D.; Ma, J.; Xu, T. Impacts of Niobia Loading on Active Sites and Surface Acidity in NbO$_x$/CeO₂−ZrO₂ NH₃−SCR Catalysts. *Appl. Catal., B* **2015**, *179*, 380−394.

(12) Li, X.; Li, J.; Peng, Y.; Zhang, T.; Liu, S.; Hao, J. Selective Catalytic Reduction of NO with NH₃ over Novel Iron−Tungsten Mixed Oxide Catalyst in a Broad Temperature Range. *Catal. Sci. Technol.* **2015**, *5*, 4556−4564.

(13) Roy, S.; Hegde, M.; Madras, G. Catalysis for NO$_x$ Abatement. *Appl. Energy* **2009**, *86*, 2283−2297.

(14) Taylor, K. C.; Schlatter, J. C. Selective Reduction of Nitric Oxide over Noble Metals. *J. Catal.* **1980**, *63*, 53−71.

(15) Cant, N. W.; Angove, D. E.; Chambers, D. C. Nitrous Oxide Formation During the Reaction of Simulated Exhaust Streams over Rhodium, Platinum and Palladium Catalysts. *Appl. Catal., B* **1998**, *17*, 63−73.

(16) Takahashi, N.; Shinjoh, H.; Iijima, T.; Suzuki, T.; Yamazaki, K.; Yokota, K.; Suzuki, H.; Miyoshi, N.; Matsumoto, S.-i.; Tanizawa, T.; et al. The New Concept 3-Way Catalyst for Automotive Lean-Burn Engine: NO$_x$ Storage and Reduction Catalyst. *Catal. Today* **1996**, *27*, 63−69.

(17) Yokota, K.; Fukui, M.; Tanaka, T. Catalytic Removal of Nitric Oxide with Hydrogen and Carbon Monoxide in the Presence of Excess Oxygen. *Appl. Surf. Sci.* **1997**, *121−122*, 273−277.

(18) Granger, P.; Dujardin, C.; Paul, J.-F.; Leclercq, G. An Overview of Kinetic and Spectroscopic Investigations on Three-Way Catalysts: Mechanistic Aspects of the CO+NO and CO+N₂O Reactions. *J. Mol. Catal. A: Chem.* **2005**, *228*, 241−253.

(19) Deng, C.; Qian, J.; Yu, C.; Yi, Y.; Zhang, P.; Li, W.; Dong, L.; Li, B.; Fan, M. Influences of Doping and Thermal Stability on the Catalytic Performance of CuO/Ce₂₀M₁O$_x$ (M = Zr, Cr, Mn, Fe, Co, Sn) Catalysts for NO Reduction by CO. *RSC Adv.* **2016**, *6*, No. 113630.

(20) Qiao, B.; Liang, J.-X.; Wang, A.; Xu, C. Q.; Li, J.; Zhang, T.; Liu, J. J. Ultrastable Single-Atom Gold Catalysts with Strong Covalent Metal-Support Interaction (CMSI). *Nano Res.* **2015**, *8*, 2913−2924.

(21) Yang, Y.; Ochoa-Hernández, C.; Víctor, A.; Pizarro, P.; Coronado, J. M.; Serrano, D. P. Effect of Metal−Support Interaction on the Selective Hydrodeoxygenation of Anisole to Aromatics over Ni-Based Catalysts. *Appl. Catal., B* **2014**, *145*, 91−100.

(22) Kast, P.; Friedrich, M.; Girgsdies, F.; Kröhnert, J.; Teschner, D.; Lunkenbein, T.; Behrens, M.; Schlögl, R. Strong Metal-Support Interaction and Alloying in Pd/ZnO Catalysts for CO Oxidation. *Catal. Today* **2016**, *260*, 21−31.

(23) Granger, P.; Dathy, C.; Lecomte, J.; Leclercq, L.; Prigent, M.; Mabilon, G.; Leclercq, G. Kinetics of the NO and CO Reaction over Platinum Catalysts: I. Influence of the Support. *J. Catal.* **1998**, *173*, 304−314.

(24) Bera, P.; Patil, K.; Jayaram, V.; Subbanna, G.; Hegde, M. Ionic Dispersion of Pt and Pd on CeO₂ by Combustion Method: Effect of Metal−Ceria Interaction on Catalytic Activities for NO Reduction and CO and Hydrocarbon Oxidation. *J. Catal.* **2000**, *196*, 293−301.

(25) Schmal, M.; Baldanza, M.; Vannice, M. A. Pd-xMo/Al₂O₃ Catalysts for NO Reduction by CO. *J. Catal.* **1999**, *185*, 138−151.

(26) Cao, Y.; Ran, R.; Wu, X.; Wu, X.; Wan, J.; Weng, D. Ageing Resistance of Rhodium Supported on CeO₂−ZrO₂ and ZrO₂: Rhodium Nanoparticle Structure and Rh−Support Interaction under Diverse Ageing Atmosphere. *Catal. Today* **2017**, *281*, 490−499.

(27) Peck, T. C.; Reddy, G. K.; Jones, M.; Roberts, C. A. Monolayer Detection of Supported Fe and Co Oxides on Ceria to Establish Structure−Activity Relationships for Reduction of NO by CO. *J. Phys. Chem. C* **2017**, *121*, 8435−8443.

(28) Broqvist, P.; Panas, I.; Persson, H. A DFT Study on CO Oxidation over Co₃O₄. *J. Catal.* **2002**, *210*, 198−206.

(29) Liotta, L.; Pantaleo, G.; Di Carlo, G.; Marcı, G.; Deganello, G. Structural and Morphological Investigation of a Cobalt Catalyst Supported on Alumina-Baria: Effects of Redox Treatments on the Activity in the NO Reduction by CO. *Appl. Catal., B* **2004**, *52*, 1−10.

(30) Deng, C.; Huang, Q.; Zhu, X.; Hu, Q.; Su, W.; Qian, J.; Dong, L.; Li, B.; Fan, M.; Liang, C. The Influence of Mn-Doped CeO₂ on the Activity of CuO/CeO₂ in CO Oxidation and NO+ CO Model Reaction. *Appl. Surf. Sci.* **2016**, *389*, 1033−1049.

(31) Hu, Y.; Dong, L.; Shen, M.; Liu, D.; Wang, J.; Ding, W.; Chen, Y. Influence of Supports on the Activities of Copper Oxide Species in the Low-Temperature NO + CO Reaction. *Appl. Catal., B* **2001**, *31*, 61−69.

(32) Ma, L.; Luo, M.-F.; Chen, S.-Y. Redox Behavior and Catalytic Properties of CuO/Ce₀.₈ Zr₀.₂O₂ Catalysts. *Appl. Catal., A* **2003**, *242*, 151−159.

(33) Nakanowatari, S.; Mei, R.; Feldt, M.; Ackermann, L. Cobalt (III)-Catalyzed Hydroarylation of Allenes Via C−H Activation. *ACS Catal.* **2017**, *7*, 2511−2515.

(34) Wang, X.; Wen, W.; Mi, J.; Li, X.; Wang, R. The Ordered Mesoporous Transition Metal Oxides for Selective Catalytic Reduction of NO$_x$ at Low Temperature. *Appl. Catal., B* **2015**, *176−177*, 454−463.

(35) Kang, M.; Song, M. W.; Lee, C. H. Catalytic Carbon Monoxide Oxidation over CoO$_x$/CeO₂ Composite Catalysts. *Appl. Catal., A* **2003**, *251*, 143−156.

(36) Kubacka, A.; Fernández-García, M.; Martínez-Arias, A. Catalytic Hydrogen Production through WGS or Steam Reforming of Alcohols over Cu, Ni and Co Catalysts. *Appl. Catal., A* **2016**, *518*, 2−17.

(37) Djinović, P.; Črnivec, I. G. O.; Pintar, A. Biogas to Syngas Conversion without Carbonaceous Deposits Via the Dry Reforming Reaction Using Transition Metal Catalysts. *Catal. Today* **2015**, *253*, 155−162.

(38) Carvalho, F. L.; Asencios, Y. J.; Bellido, J. D.; Assaf, E. M. Bio-Ethanol Steam Reforming for Hydrogen Production over Co₃O₄/CeO₂ Catalysts Synthesized by One-Step Polymerization Method. *Fuel Process. Technol.* **2016**, *142*, 182−191.

(39) Yang, Q.; Gu, F.; Tang, Y.; Zhang, H.; Liu, Q.; Zhong, Z.; Su, F. A Co₃O₄−CeO₂ Functionalized SBA-15 Monolith with a Three-Dimensional Framework Improves NO$_x$-Assisted Soot Combustion. *RSC Adv.* **2015**, *5*, 26815−26822.

(40) An, K.; Alayoglu, S.; Musselwhite, N.; Plamthottam, S.; Melaet, G. M.; Lindeman, A. E.; Somorjai, G. A. Enhanced CO Oxidation Rates at the Interface of Mesoporous Oxides and Pt Nanoparticles. *J. Am. Chem. Soc.* **2013**, *135*, 16689−16696.

(41) Jansson, J.; Palmqvist, A. E.; Fridell, E.; Skoglundh, M.; Österlund, L.; Thormählen, P.; Langer, V. On the Catalytic Activity of Co₃O₄ in Low-Temperature CO Oxidation. *J. Catal.* **2002**, *211*, 387−397.

(42) Ozawa, M.; Takahashi-Morita, M.; Kobayashi, K.; Haneda, M. Core-Shell Type Ceria Zirconia Support for Platinum and Rhodium Three Way Catalysts. *Catal. Today* **2017**, *281*, 482−489.

(43) Xu, W.; Yu, Y.; Zhang, C.; He, H. Selective Catalytic Reduction of NO by NH₃ over a Ce/TiO₂ Catalyst. *Catal. Commun.* **2008**, *9*, 1453−1457.

(44) Deng, C.; Li, B.; Dong, L.; Zhang, F.; Fan, M.; Jin, G.; Gao, J.; Gao, L.; Zhang, F.; Zhou, X. NO Reduction by CO over CuO Supported on CeO₂-Doped TiO₂: The Effect of the Amount of a Few CeO₂. *Phys. Chem. Chem. Phys* **2015**, *17*, 16092−16109.

(45) Chen, L.; Si, Z.; Wu, X.; Weng, D. Drift Study of CuO−CeO₂−TiO₂ Mixed Oxides for NO$_x$ Reduction with NH₃ at Low Temperatures. *ACS Appl. Mater. Interfaces* **2014**, *6*, 8134−8145.

(46) Tian, D.; Zeng, C.; Fu, Y.; Wang, H.; Luo, H.; Xiang, C.; Wei, Y.; Li, K.; Zhu, X. A DFT Study of the Structural, Electronic and Optical Properties of Transition Metal Doped Fluorite Oxides: Ce₀.₇₅M₀.₂₅O₂ (M = Fe, Co, Ni). *Solid State Commun.* **2016**, *231*, 68−79.

(47) Konsolakis, M.; Sgourakis, M.; Carabineiro, S. A. Surface and Redox Properties of Cobalt–Ceria Binary Oxides: On the Effect of Co Content and Pretreatment Conditions. *Appl. Surf. Sci.* **2015**, *341*, 48–54.

(48) Liu, N.; Chen, X.; Zhang, J.; Schwank, J. W. Drifts Study of Photo-Assisted Catalytic CO+NO Redox Reaction over CuO/CeO_2-TiO_2. *Catal. Today* **2015**, *258*, 139–147.

(49) Wachs, I. E. Raman and Ir Studies of Surface Metal Oxide Species on Oxide Supports: Supported Metal Oxide Catalysts. *Catal. Today* **1996**, *27*, 437–455.

(50) Barton, D. G.; Shtein, M.; Wilson, R. D.; Soled, S. L.; Iglesia, E. Structure and Electronic Properties of Solid Acids Based on Tungsten Oxide Nanostructures. *J. Phys. Chem. B* **1999**, *103*, 630–640.

(51) Jehng, J. M.; Wachs, I. E. Molecular Structures of Supported Niobium Oxide Catalysts under In-situ Conditions. *J. Phys. Chem.* **1991**, *95*, 7373–7379.

(52) Savereide, L.; Nauert, S. L.; Roberts, C. A.; Notestein, J. M. The Effect of Support Morphology on CoO_x/CeO_2 Catalysts for the Reduction of NO by CO. *J. Catal.* **2018**, *366*, 150–158.

(53) Luisetto, I.; Tuti, S.; Di Bartolomeo, E. Co and Ni Supported on CeO_2 as Selective Bimetallic Catalyst for Dry Reforming of Methane. *Int. J. Hydrogen Energy* **2012**, *37*, 15992–15999.

(54) Ay, H.; Üner, D. Dry Reforming of Methane over CeO_2 Supported Ni, Co and Ni–Co Catalysts. *Appl. Catal., B* **2015**, *179*, 128–138.

(55) Xue, L.; Zhang, C.; He, H.; Teraoka, Y. Catalytic Decomposition of N_2O over CeO_2 Promoted Co_3O_4 Spinel Catalyst. *Appl. Catal., B* **2007**, *75*, 167–174.

(56) Clausen, B.; Steffensen, G.; Fabius, B.; Villadsen, J.; Feidenhans, R.; Topsøe, H. In-situ Cell for Combined XRD and On-line Catalysis Tests: Studies of Cu-Based Water Gas Shift and Methanol Catalysts. *J. Catal.* **1991**, *132*, 524–535.

(57) Sarkar, B.; Goyal, R.; Pendem, C.; Sasaki, T.; Bal, R. Highly Nanodispersed Gd-Doped Ni/ZSM-5 Catalyst for Enhanced Carbon-Resistant Dry Reforming of Methane. *J. Mol. Catal. A: Chem.* **2016**, *424*, 17–26.

(58) Zhang, Q.; Zhang, T.; Shi, Y.; Zhao, B.; Wang, M.; Liu, Q.; Wang, J.; Long, K.; Duan, Y.; Ning, P. A Sintering and Carbon-Resistant Ni-SBA-15 Catalyst Prepared by Solid-State Grinding Method for Dry Reforming of Methane. *J. CO_2 Util.* **2017**, *17*, 10–19.

(59) Kleitz, F.; Choi, S. H.; Ryoo, R. Cubic Ia3d Large Mesoporous Silica: Synthesis and Replication to Platinum Nanowires, Carbon Nanorods and Carbon Nanotubes. *Chem. Commun.* **2003**, 2136–2137.

(60) Natile, M. M.; Glisenti, A. CoO_x/CeO_2 Nanocomposite Powders: Synthesis, Characterization, and Reactivity. *Chem. Mater.* **2005**, *17*, 3403–3414.

(61) Kim, T.; Burrows, A.; Kiely, C. J.; Wachs, I. E. Molecular/Electronic Structure–Surface Acidity Relationships of Model-Supported Tungsten Oxide Catalysts. *J. Catal.* **2007**, *246*, 370–381.

(62) Kim, T.; Wachs, I. E. CH_3OH Oxidation over Well-Defined Supported V_2O_5/Al_2O_3 Catalysts: Influence of Vanadium Oxide Loading and Surface Vanadium–Oxygen Functionalities. *J. Catal.* **2008**, *255*, 197–205.

(63) Agarwal, S.; Zhu, X.; Hensen, E.; Lefferts, L.; Mojet, B. Defect Chemistry of Ceria Nanorods. *J. Phys. Chem. C* **2014**, *118*, 4131–4142.

(64) Yu, T.; Zhu, Y.; Xu, X.; Shen, Z.; Chen, P.; Lim, C. T.; Thong, J. L.; Sow, C. H. Controlled Growth and Field-Emission Properties of Cobalt Oxide Nanowalls. *Adv. Mater.* **2005**, *17*, 1595–1599.

(65) Wu, Z.; Li, M.; Howe, J.; Meyer, H. M., III; Overbury, S. H. Probing Defect Sites on CeO_2 Nanocrystals with Well-Defined Surface Planes by Raman Spectroscopy and O_2 Adsorption. *Langmuir* **2010**, *26*, 16595–16606.

(66) Reddy, B. M.; Khan, A.; Yamada, Y.; Kobayashi, T.; Loridant, S.; Volta, J.-C. Structural Characterization of CeO_2– TiO_2 and V_2O_5/CeO_2–TiO_2 Catalysts by Raman and XPS Techniques. *J. Phys. Chem. B* **2003**, *107*, 5162–5167.

(67) Hadjiev, V.; Iliev, M.; Vergilov, I. The Raman Spectra of Co_3O_4. *J. Phys. C: Solid State Phys.* **1988**, *21*, L199.

(68) Iwanek, E.; Krawczyk, K.; Petryk, J.; Sobczak, J. W.; Kaszkur, Z. Direct Nitrous Oxide Decomposition with CoO_x-CeO_2 Catalysts. *Appl. Catal., B* **2011**, *106*, 416–422.

(69) Cónsul, J. M. D.; Costilla, I.; Gigola, C. E.; Baibich, I. M. NO Reduction with CO on Alumina-Modified Silica-Supported Palladium and Molybdenum-Palladium Catalysts. *Appl. Catal., A* **2008**, *339*, 151–158.

(70) Lee, Y.-L.; Jha, A.; Jang, W.-J.; Shim, J.-O.; Rode, C. V.; Jeon, B.-H.; Bae, J. W.; Roh, H.-S. Effect of Alkali and Alkaline Earth Metal on Co/CeO_2 Catalyst for the Water-Gas Shift Reaction of Waste Derived Synthesis Gas. *Appl. Catal., A* **2018**, *551*, 63–70.

(71) de Souza, P. M.; Rabelo-Neto, R. C.; Borges, L. E.; Jacobs, G.; Davis, B. H.; Resasco, D. E.; Noronha, F. B. Hydrodeoxygenation of Phenol over Pd Catalysts. Effect of Support on Reaction Mechanism and Catalyst Deactivation. *ACS Catal.* **2017**, *7*, 2058–2073.

(72) Pinton, N.; Vidal, M.; Signoretto, M.; Martinez-Arias, A.; Corberán, V. C. Ethanol Steam Reforming on Nanostructured Catalysts of Ni, Co and CeO_2: Influence of Synthesis Method on Activity, Deactivation and Regenerability. *Catal. Today* **2017**, *296*, 135–143.

(73) Jansson, J.; Skoglundh, M.; Fridell, E.; Thormählen, P. A Mechanistic Study of Low Temperature CO Oxidation over Cobalt Oxide. *Top. Catal.* **2001**, *16*, 385–389.

(74) Smith, W.; Hobson, A. The Structure of Cobalt Oxide, Co_3O_4. *Acta Crystallogr., Sect. B: Struct. Crystallogr. Cryst. Chem.* **1973**, *29*, 362–363.

(75) Greenwald, S. A. The Antiferromagnetic Structure Deformations in CoO and MnTe. *Acta Crystallogr.* **1953**, *6*, 396–398.

(76) Li, C.; Sakata, Y.; Arai, T.; Domen, K.; Maruya, K.-i.; Onishi, T. Carbon Monoxide and Carbon Dioxide Adsorption on Cerium Oxide Studied by Fourier-Transform Infrared Spectroscopy. Part 1.—Formation of Carbonate Species on Dehydroxylated CeO_2, at Room Temperature. *J. Chem. Soc., Faraday Trans. 1* **1989**, *85*, 929–943.

(77) Yao, X.; Yu, Q.; Ji, Z.; Lv, Y.; Cao, Y.; Tang, C.; Gao, F.; Dong, L.; Chen, Y. A Comparative Study of Different Doped Metal Cations on the Reduction, Adsorption and Activity of $CuO/Ce_{0.67}M_{0.33}O_2$ (M = Zr^{4+}, Sn^{4+}, Ti^{4+}) Catalysts for NO+CO Reaction. *Appl. Catal., B* **2013**, *130–131*, 293–304.

(78) Sun, C.; Zhu, J.; Lv, Y.; Qi, L.; Liu, B.; Gao, F.; Sun, K.; Dong, L.; Chen, Y. Dispersion, Reduction and Catalytic Performance of Cuo Supported on ZrO_2-Doped TiO_2 for NO Removal by CO. *Appl. Catal., B* **2011**, *103*, 206–220.

(79) Liu, L.; Liu, B.; Dong, L.; Zhu, J.; Wan, H.; Sun, K.; Zhao, B.; Zhu, H.; Dong, L.; Chen, Y. In Situ FT-Infrared Investigation of CO or/and NO Interaction with $CuO/Ce_{0.67}Zr_{0.33}O_2$ Catalysts. *Appl. Catal., B* **2009**, *90*, 578–586.

(80) Yao, X.; Xiong, Y.; Zou, W.; Zhang, L.; Wu, S.; Dong, X.; Gao, F.; Deng, Y.; Tang, C.; Chen, Z.; et al. Correlation between the Physicochemical Properties and Catalytic Performances of $Ce_xSn_{1-x}O_2$ Mixed Oxides for NO Reduction by CO. *Appl. Catal., B* **2014**, *144*, 152–165.

(81) Chen, T.-y.; Su, J.; Zhang, Z.; Cao, C.; Wang, X.; Si, R.; Liu, X.; Shi, B.; Xu, J.; Han, Y.-F. Structure Evolution of CO–CoO_x Interface for Higher Alcohol Synthesis from Syngas over Co/CeO_2 Catalysts. *ACS Catal.* **2018**, *8*, 8606–8617.

(82) Deng, C.; Li, M.; Qian, J.; Hu, Q.; Huang, M.; Lin, Q.; Ruan, Y.; Dong, L.; Li, B.; Fan, M. A Study of Different Doped Metal Cations on the Physicochemical Properties and Catalytic Activities of $Ce_{20}M_1O_x$ (M = Zr, Cr, Mn, Fe, Co, Sn) Composite Oxides for Nitric Oxide Reduction by Carbon Monoxide. *Chem. — Asian J.* **2016**, *11*, 2144–2156.